



Earth transformed: detailed mapping of global human modification from 1990 to 2017

David M. Theobald^{1,2}, Christina Kennedy³, Bin Chen⁴, James Oakleaf³, Sharon Baruch-Mordo³, Joe Kiesecker³

¹Conservation Planning Technologies, Fort Collins, CO 80521, USA

²Department of Fish, Wildlife, and Conservation Biology, Colorado State University, Fort Collins, CO 80523, USA

³Global Lands Program, The Nature Conservancy, Fort Collins, CO 80524, USA

⁴Department of Land, Air and Water Resources, University of California, Davis, CA 95616, USA

Correspondence to: David M. Theobald, Ph.D. (dmt@davidmtheobald.com)



Abstract

Data on the extent, patterns, and trends of human land use are critically important to support global and national priorities for conservation and sustainable development. To inform these issues, we created a series of detailed global datasets for 1990, 2000, 2010, and 2015 to evaluate temporal and spatial trends of land use modification of terrestrial lands (excluding Antarctica). We found that the expansion and increase of human modification between 1990 and 2015 resulted in 1.6 M km² of natural land lost. The percent change between 1990 and 2015 was 15.2% or 0.61% annually – roughly 178 km² daily. Over the pause of a deep breath, over 8 football pitches of natural lands were lost (~17 per minute). Worryingly, we found that the global rate of loss has increased over the past 25 years. The greatest loss of natural lands from 1990-2015 occurred in Oceania, Asia, and Europe, and the biomes with the greatest loss were mangroves, tropical & subtropical moist broadleaf forests, and tropical & subtropical dry broadleaf forests. We also created a contemporary (~2017) estimate of human modification that included additional stressors and found that globally 14.5% or 18.5 M km² of lands have been completely modified – an area greater than Russia. Our novel datasets are detailed (0.09 km² resolution), temporal (1990-2015), recent (~2017), comprehensive (11 change stressors, 14 current), robust (using an established framework and incorporating classification errors and parameter uncertainty), and strongly validated. We believe these datasets will support better understanding of the profound transformation wrought by human activities and provide foundational data on the amounts, patterns, and rates of change to inform planning and decision making for environmental mitigation, protection, restoration, and adaptation to climate change. The datasets generated from this work are available at <https://doi.org/10.5061/dryad.n5tb2rbs1> (Theobald et al. 2020).



1 Introduction

40 Humans have transformed the earth in profound ways (Marsh 1885; Jordan et al. 1990; Vitousek et al.
1997), contributing to global climate change (IPCC 2019), causing global habitat loss and
fragmentation, and contributing to declines in biodiversity and critical ecosystem services (IPBES
2019). Addressing the consequences of rapid habitat loss and land use change are essential for
45 implementation of various international initiatives, including the Convention on Biological Diversity
2020 Aichi Biodiversity targets, the United Nations 2030 Sustainable Development Goals (esp. Goal
15; Secretariat of the Convention on Biological Diversity, 2010), the Bonn Challenge (Verdone & Seidl,
2017), and the Global Deal for Nature (Dinerstein et al. 2019). Foundational to addressing these goals
is a firm understanding of the rates, trends, and amount of these land use changes. Efforts to date
(Klein Goldewijk et al. 2007; Venter et al. 2016; Geldman et al. 2019; Kennedy et al. 2019a) have been
50 limited due to the unavailability of contemporary, temporally comparable, and high-resolution data.

Here we describe a new dataset that maps the degree of human modification of terrestrial
ecosystems globally, for recent changes from 1990 to 2015, and for contemporary (circa 2017)
conditions. We mapped human activities that directly or indirectly alter natural systems, which we
55 call anthropogenic drivers of ecological stress or “stressors” (following Salafsky et al., 2008;
Theobald 2013). Similar to other efforts (Sanderson et al. 2002; Theobald 2010, 2013; Geldmann et al.
2014; Venter et al. 2016; Kennedy et al. 2019a), we augmented remotely-sensed data with
traditionally-mapped cartographic features. This is because remotely sensed imagery has limitations
for this application – especially prior to ~2010 – including obstructions by vegetation canopy (e.g.,
60 some roads, trails), inability to detect small or narrow features (e.g., towers, wind turbines,
powerlines), or can require human-interpretation to classify efficiently.

We mapped the degree of human modification based on an established approach that has been
applied nationally, internationally, and globally (Theobald 2010, 2013; Gonzalez-Abraham et al. 2015;
65 Kennedy et al. 2019a). It uses an existing classification system (Salafsky et al., 2008) to: (a) ensure
parsimony; (b) distinguish two spatial components (area of use and intensity of use); (c) use a
physically-based measure that is needed to estimate change (Gardner and Urban 2007); (d)
incorporate spatial and classification uncertainty; and (e) combine multiple stressors into an overall
measure that assumes additive but monotonic relationships and addresses the correlation among
70 variables (Theobald 2010). The resulting quantitative estimate of human modification has values
ranging from 0 to 1 that support robust landscape assessments (Schultz 2001; Hajkowicz and Collins
2007).

To understand temporal landscape change, we calculated the degree of human modification –
75 denoted by H – for the years 1990, 2000, 2010, and 2015 using methods and datasets that minimize
noise and bias. Second, we included additional stressors not incorporated previously, including
disturbance of natural processes due to reservoirs, effects from air pollution, and human intrusion
(Theobald 2008). Third, we calculated human stressors using up to two orders of magnitude finer
resolution data (0.09 vs. 1-86 km²) than past efforts (Ellis and Ramankutty 2008; Geldmann et al.



80 2014; Haddad et al. 2015; Venter et al. 2016; Geldmann et al. 2019b; Kennedy et al. 2019a). This higher
resolution reduces the loss of information of the spatial pattern within a pixel, better identifies rare
features, facilitates the application of these data for species and ecological processes that often
occur at a fine-scale, and improves the utility and relevance of these products for policy makers,
85 decision makers, and land use managers.

85 Calculating H as a real value across the full gradient of landscape changes is valuable because it can
be applied rigorously to a variety of questions, including discerning the heterogeneity of human uses
that are often lumped within broad classes like “urban”, capturing the extent and pattern of the
agricultural lands typically occurring beyond urban centers and protected areas, and delineating
90 areas of low modification – all of which are useful for conservation prioritization and planning efforts
(Kennedy et al. 2019a, 2019b). Here, we describe the technical methods and briefly report on results
on the temporal trends and current spatial patterns of human modification across all terrestrial
lands, biomes and ecoregions (Dinerstein et al. 2017). Because conservation organizations often use
this type of data to focus their activities on specific regions (e.g., Jantke et al. 2019), we provide
95 rankings by biome and ecoregion and briefly compare our results to other available results.

2 Methods

2.1 Overview

100 We calculated the degree of human modification using the Direct Threats Classification v2 (Salafsky
et al. 2008; cmp-openstandards.org), which defines a stressor as the proximate human activities or
processes that have caused, are causing, or may cause impacts on biodiversity and ecosystems. Table
1 lists the specific stressors and data sources we included in our maps: urban/built-up, crop and
pasture lands, livestock grazing, oil and gas production, mining and quarrying, power generation
(renewable and non-renewable), roads, railways, power lines and towers, logging and wood
105 harvesting, human intrusion, reservoirs, and air pollution.

110 To estimate *temporal change* in H from 1990 to 2015, we followed criteria established (Geldmann et
al. 2014) and included 11 stressors for which we could obtain global data with fine-grained resolution
($<1 \text{ km}^2$), and that provided consistent and comparable repeated measurements, especially in
regards to the data source, methods used, and appropriate time frame (Table 1). We included current
major roads and railways as a static layer in the temporal maps because in most cases some form of
road existed prior to our baseline year of 1990 (except for the relatively rare, though important, new
highway constructed).

115 To estimate the *current* amount of H circa 2017 year (median=2017, min=2012, max=2019), we included
three additional stressors, including grazing, oil and gas wells, and powerlines. We note that we were
not able to map stressors for invasive species or pathogens and genes, geologic events, or climate
change. This was because suitable temporal global data were not available to capture stressors due
to invasive species or pathogens and genes; the majority of geological events are not directly caused



120 by humans; and climate change is better modeled as separate process distinct from the effects of
direct human activities and has a plethora of research on this topic (Geldmann et al. 2014; Titeux et
al. 2016).

For each stressor s we quantified the degree of human modification as:

$$H_s = F_s * p(C_s) * I_s, \quad (1)$$

125 where F is the proportion of a pixel occupied (i.e. the footprint) by stressor s , $p(C_s)$ is the probability
that a stressor occurs at a location to account for spatial and classification uncertainty, and I is the
intensity. Importantly, F and I have a direct physical interpretation (Gardner and Urban 2007), are
well-bounded and range from 0-1, and values are a “real” data-type. Consequently, H provides the
basis for unambiguous interpretation to assess landscape change (Hajkowicz and Collins 2007;
130 Riitters et al. 2009). Specific formulas used to map raw stressor data as indicator layers are provided
below. Table 2 details our estimates of intensity values for each stressor (modified from Theobald
2013 and Kennedy et al. 2019a), which is used to differentiate land uses that have varying impacts on
terrestrial systems (e.g., grazing is less intensive than mining). Our intensity values were informed by
standardized measures of the amount of non-renewable energy required to maintain human
135 activities (Brown and Vivas 2005) and found to generally correlate with species responses to land use
where examined (Kennedy et al. 2019a).

We generated datasets that represent temporal changes between 1990 and 2015 and for current
(~2017) conditions by combining stressor layers using the fuzzy algebraic sum (Bonham-Carter, 1994;
140 Malczewski 1999; Theobald 2013), which is calculated as:

$$H = 1 - \prod_{s=1}^n (1 - H_s), \quad (2)$$

where n is the number of stressors (s) included. Of critical importance, the fuzzy sum formula is an
increasing function that calculates the cumulative effects of multiple stressors in a way that
minimizes the bias associated with non-independent stressors and assumes that multiple stressors
145 accumulate (Theobald 2010, 2013; Kennedy et al. 2019a). This differs substantially from simple
additive calculations that are commonly used (Halpern et al. 2008; Halpern and Fujita 2013; Venter et
al. 2016), but assume that stressors are independent and results in a metric that is sensitive to the
number of stressors included in the model (Malczewski 1999).

150 We mapped human modification of all terrestrial lands (excluding Antarctica) and included lands
inundated by reservoirs, but excluded other rivers and lakes. An often overlooked but critical aspect
to understand human modification is how water is mapped, especially for the interface between land
and coastlines, lakes, reservoirs, and large rivers. We mapped non-reservoir areas dominated by
water (i.e., oceans, lakes, reservoirs, and rivers) by processing data on ocean from the European
155 Space Agency’s Climate Change Initiative program (ESA CCI; 150 m, circa 2000) and surface waters
using the Global Surface Water dataset (GSW; 30 m; Pekel et al. 2016). We identified inland water
bodies (i.e. lakes, reservoirs, rivers, etc.) using ESA CCI non-ocean pixels that were at least 1 km
interior of the land-ocean interface. We identified interior water pixels using GSW with at least 75%
water occurrence from 1984-2019 and that were at least 0.0225 km² in area (to remove small lakes,



160 ponds, and narrow streams). As a result, inland water bodies and the ocean-land interface are much clearer, more consistent, and better aligned.

We summarized our estimates of human modification across all terrestrial lands, biomes, and ecoregions (defined by Dinerstein et al. 2017) and here report median (H_{med}) and mean (H_{mean}) statistics. We summarized results of temporal trends using the mean annualized difference (H_{mad}), calculated as the mean value across each analytical unit (e.g., biomes, ecoregions) of the annualized difference assuming a linear trend (H_{ad}):

$$H_{ad} = (H_u - H_t) / (u - t), \quad (3)$$

165 where u and t are the years of the datasets (e.g., $u=2015$, $t=1990$) and $u>t$. When discussing trends between 1990 and 2015, we emphasize the mean statistic because it better captures locations where H values have changed (mostly increasing over time), partly due to land uses with high values (e.g., urbanization ~ 0.8) that are not well represented in the median statistic. We calculated the increase in H , or conversely the amount of natural habitat loss, as the per-pixel value times the pixel area, summed across a given unit of analysis. This assumes that any increase in the level of human
170 modification causes natural land loss regardless of the original H level. We also report the median statistic because, as is typical of spatial landscape data, the distribution of H values is skewed to the right. Finally, we compared our results of H_{mad} to those calculated on the Human Footprint (HF for 1993-2009; Venter et al. 2016) and the temporal human pressure index (THPI for 1995-2010; Geldmann et al. 2019b).

175

180 2.2 Stressors mapped

2.2.1 Urban and built-up

To map built-up areas that are typically found in urban areas and dominated by residential, commercial, and industrial land uses, we used the most recent version of the Built-up Grid from the Global Human Settlements Layers dataset (GHSL R2018A; Pesaresi et al. 2015). The degree of human
185 modification that is contributed by built-up areas, H_{bu} , is:

$$H_{bu} = F_{bu} * p(C_{bu}) * I_{bu}, \quad (4)$$

where F_{bu} measures the proportion of the area of a pixel classified as built-up, $p(C_{bu})$ applies the GHSL-reported confidence mask (for 2014) for locations of the built-up areas (for the target year; Pesaresi et al. 2015) and I_{bu} is the intensity factor specified in Table 2.

190

2.2.2 Agriculture

We mapped agriculture stressors by identifying land cover classes associated with crop and pastureland from ESA CCI land cover datasets (ESA CCI 2015; Perez-Hoyos et al. 2017; Li et al. 2018) available at 0.09 km² for 1992, 2000, 2010, and 2015. We merged the cropland and pastureland stressors because these two classes are combined in the ESA land cover data, and they are
195 challenging to distinguish even at higher resolution (~ 30 m, Wickham et al. 2017). To incorporate classification errors associated with all cover classes, we multiplied the footprint $F_{cp} = 1.0$ times the probability $p(C_{cp})$ that a pixel with cover class C was found to be cropland or pasture, C_{cp} , by interpreting reported accuracy assessment results (ESA CCI 2017, in Table 3). To reduce the effects of



200 scattered pixels that have some probability of being mapped as cropland-pastureland (e.g.,
misclassified pixels high-elevation tundra or alpine areas), we multiplied $p(C_{cp})$ by the proportion of
lands estimated to be in crops from the Unified Cropland Layer (Waldner et al. 2016), v so that:

$$p(C_{cp})' = p(C_{cp}) \times v, \quad (5)$$

and also reduced the value of $p(C_{cp})'$ based on patch size A , assuming that accuracy declines rapidly
with cropland/pastureland small “patches” ($A < 1 \text{ km}^2$) using:

205
$$p(C_{cp})'' = (p(C_{cp})')^2, A < 1. \quad (6)$$

We then calculated H_{cp} as:

$$H_{cp} = F_{cp} * p(C_{cp})'' * I_{cp}. \quad (7)$$

210 We developed spatially-explicit estimates of agricultural intensity based on land management, such
as cropping and number of rotations, tilling, and cutting operations because these activities typically
vary geographically (van asselen and Verburg 2012; Kehoe et al. 2017). We followed existing methods
(Chaudhary and Brooks 2018) to estimate three intensities of agricultural land use – minimal, light,
and intense – and then mapped them using cover types from Global Land Systems v2 dataset (GLS;
215 Kehoe et al. 2017) by estimating intensity values (I) for each of the agricultural intensity types (Table
2). Although GLS v2 represents conditions circa 2005, we incorporated temporal changes by
weighting the proportion of agricultural lands from the time-varying ESA CCI land cover datasets.

To estimate the modification associated with the grazing of domestic livestock (H_{au}), we used the
220 Gridded Livestock of the World v3 (Robinson et al. 2014; Gilbert et al. 2018a, Gilbert et al. 2018b) that
maps the density of animals per km^2 (G) for eight types of livestock (j): buffaloes, cattle, chickens,
ducks, goats, horses, pigs, and sheep. To calculate the overall footprint of grazing (F_{au}), we summed
the weighted densities by global averages of livestock unit (LU) coefficients ($w_i = 0.84, 0.67, 0.01,$
0.01, 0.10, 0.84, 0.23, 0.10, listed respectively for each livestock species stated above). We used a
225 lower threshold found at 10% to remove values $< 1.0 \text{ LUs/km}^2$ (similar to Jacobson et al. 2019) and
1000 LU km^2 as an upper threshold because it is a common breakpoint between grazing and
industrial feedlots (Gerber et al. 2010). We assumed (here, and below unless otherwise provided) no
uncertainty ($p(C_{au}) = 1.0$), because we lacked explicit data to do so. We then \log_{10} transformed and
max-normalized (Kennedy et al. 2019a) to obtain 0-1 values, and calculated the mean H_{au} using a 10
km radius moving window to reduce the effects of the coarser-resolution pixels:

230
$$F_{au} = \sum_{j=1}^8 G_j w_j, \max(1000), \min(1) \quad (8)$$

$$H_{au} = ((\log(F_{au} + 1)) / \log(1000)) * p(C_{au}) * I_{au}. \quad (9)$$

2.2.3 Energy and extractive resources

235 To estimate stressors associated with extractive energy production, we mapped gas flares derived
from “night-time lights” using data from the Visible Infrared Imaging Radiometer Suite from the
Suomi National Polar-orbiting Partnership (VIIRS; Elvidge et al. 2013). Roughly 90% of gas flares occur
at locations where oil and gas are extracted (Elvidge et al. 2015). We used point data processed
specifically to identify gas flares in VIIRS for 2012/2013 (Elvidge et al. 2016). For each flare, we
approximated a footprint of 0.057 km^2 per well head (Allred et al. 2015). It is common to



240 approximate the footprint of points (and lines) using a simple “buffer”, which implicitly assumes no
 location error and no distance-decay from the point of origin. Such a buffer approach essentially
 centers a cylinder on each data point, where volume (V) equals the approximate footprint and height
 (h) and a perfect certainty of 1.0. Here, however, we assumed some uncertainty in the location of the
 point and that the effects associated with a feature such as an oil/gas well-head diminish with
 245 distance. That is, rather than use a cylinder with volume V (or similarly a simple uniform buffer away
 from linear features, e.g. powerlines or roads), we used a conic shaped kernel centered on the point
 to calculate the uncertainty $p(C_{og})$, where the height of the cone $h=0.5$ represents a conservative
 estimate of spatial accuracy (Theobald 2013). We derived the cone radius $D=0.329$ km by setting V to
 the footprint of 0.057 km²:

$$D = \sqrt{(3/h) V / \pi} , \quad (10)$$

250 Thereby the uncertainty parameter for each point is calculated using:

$$p(C_{og}) = 3h/\pi D^2 . \quad (11)$$

We assigned the value of $p(C_{og})$ that overlapped the center of each pixel, with $\max p(C_{og}) = 1.0$.
 Human modification was then calculated as:

$$H_{og} = F_{og} * p(C_{og}) * I_{og} . \quad (12)$$

255

2.2.5 Mines and quarries

To estimate modification due to mines and quarries, we derived locations represented as points from
 a global mining dataset ($n=34,565$; S&P 2018; Valenta et al. 2019). We retained surface mines that
 were constructed, construction started, in operation, in the process of being commissioned, or
 residual production ($n=22,705$). For the temporal change analysis, we removed locations that did not
 260 have a specified year of construction ($n=3,634$). We calculated the mean disturbed area and
 associated infrastructure of a mine by intersecting mine point locations with 441,623 polygons that
 represent footprints of quarries/mines (OpenStreetmap, 2016). For four types of mines: coal;
 hard-rock (bauxite, cobalt, copper, gold, iron ore, lead, manganese, molybdenum, nickel, phosphate,
 platinum, silver, tin, U_3O_8 , and zinc); diamonds; and other (antimony, chromite, graphite, ilmenite,
 265 lanthanides, lithium, niobium, palladium, tantalum, and tungsten), we estimated the mean area (a)
 to be: 12.95 km² ($n=647$) for coal, 8.54 km² ($n=860$) for hard-rock, 5.21 km² ($n=39$) for diamonds, and 3.40
 km² ($n=27$) for other. Finally, following equations 8 and 9, we calculated $p(C_m)$ for each of the four
 mining types using D of 4.973, 4.038, 2.548, and 3.154 km, respectively, and calculated H_m as:

$$H_m = F_m * p(C_m) * I_m . \quad (13)$$

270

2.2.6 Power plants

To estimate the effects of where energy is produced, we mapped the location of power plants
 represented as points ($n=29,903$; WRI 2019). For the temporal change analysis, we removed locations
 that did not have a specified year of construction ($n=16,288$). We estimated $p(C_{pp})$ using a
 conic-shaped kernel (Eqs. 8 and 9) and $h=0.5$. We mapped both non-renewable energy forms (H_{ppn} ;
 275 coal, oil, natural gas) and renewable energy forms (H_{ppr} ; geothermal, hydro, solar, wind), where we
 assumed $F_{pp}=1$ and calculated a single $p(C_{pp})$ for both non-renewable and renewable energy sectors
 with $D_{pp}=1224$ m (following Theobald 2013):

$$H_{ppn} = F_{pp} * p(C_{ppn}) * I_{ppn} , \quad (14)$$



$$H_{ppr} = F_{pp} * p(C_{ppr}) * I_{ppr} \quad (15)$$

280

2.2.7 Transportation and service corridors

For transportation, we mapped roads and railways using OpenStreetMap highway linear features (OpenStreetMap, 2019). We calculated the footprint for the following transportation types: major (motorway, primary, secondary, trunk, link), minor (residential, tertiary, tertiary-link), two-track roads and railways as:

285

$$F_{rr} = \sum_{i=0}^c (w / \alpha) * \mu, \quad (16)$$

$$H_{rr} = F_{rr} * p(C_{rr}) * I_{rr}, \quad (17)$$

290

where w is the estimated width of a road of type i from Table 2, α is the pixel width (i.e. 300 m), and $\mu=0.79$ to adjust for the fractal dimension of road lines crossing cells (Theobald 2000) because road lines often cross pixels at random angles. If a divided highway is represented as two separate lines, then each is represented independently. Also, if a cell has two or more roadway types cross it (e.g., where a secondary road joins a highway), the fuzzy sum of H_{rr} for both roads is calculated. Note that use of roads is incorporated into the “human intrusion” stressor (described below).

295

To map the modification associated with above-ground powerlines (H_{pl}), we used:

$$H_{pl} = F_{pl} * p(C_{pl}) * I_{pl}, \quad (18)$$

where F_{pl} is calculated using a 500 m buffer (Theobald 2013), and $p(C_{pl})$ is calculated using $h=0.5$, and I_{pl} is the estimate of intensity.

300

To estimate a stressor associated with electrical infrastructure and energy use (H_{nl}), we mapped “night-time lights” using the Defense Meteorological Satellite Program/Operational Linescan System (DMSP/OLS; Elvidge et al., 2001) “stable” lights dataset. We included this as a distinct stressor from the energy extraction stressor (oil and gas flares, discussed above) because gas flares are derived by finding anomalies (high values) in the images rather than from the “stable lights” product, and the footprints associated with the flares are an extremely small fraction of the overall extent of energy infrastructure.

305

To maximize temporal consistency, we used the intercalibrated DMSP/OLS dataset (Zhang et al. 2016; Li and Zhou 2017) and extended their approach for 2013 (using $a=1.01$, $b=0.00882$, $c=-0.965$; Zhang et al. 2016). DMSP/OLS values, L , are expected to range from 0 to 63, but because max values differed yearly (ranging from 57.87 - 66.16), we normalized all images (1992-2013) to range from 0 to 1.0 using the max-adjusted value for each year (L'). To reduce the effects of noise in the images in areas with low-light and in high northerly latitudes, we removed nighttime light values when $L' < 0.077$ – that is, we set values to *null* when they were below the 25th percentile of the global terrestrial distribution compared to the often used noise threshold of $L=5$ (following Elvidge et al. 2001).

315

To adjust for inter-annual spatial-misalignment errors (Elvidge et al. 2013), we adjusted the normalized DMSP image for 2013 to align with the 2013 VIIRS product by identifying sharply contrasting and consistent signals at 10 locations ($n=10$) distributed across the continents. We then



320 visually compared each of the images from 1992-2012 to the DMSP image for 2013 and shifted the
images to align them (averaged shift in meters: $x=359.5, y=476.2$). To further reduce inter-annual
variability, we averaged image values at each pixel using a 3-year “tail” and used a
rank-ordered-centroid weighting (Roszkowska 2013) such that the spatially-aligned and
temporally-smoothed nightlight value Y for year t is:

$$325 \quad Y_t = (L'_t * 0.62) + (L'_{t-1} * 0.26) + (L'_{t-2} * 0.12) \cdot \quad (19)$$

Finally, to reduce the blooming effects and to take advantage of the higher-quality VIIRS-based
nightlights (i.e. higher spatial resolution, reduction of saturated pixels), we sharpened DMSP
nightlight values y_t using the VIIRS brightness value y to be proportional to the ratio of the DMSP
values:

$$330 \quad Y'_t = Y_t * (L'_t \div L_{2013}) \cdot \quad (20)$$

We then transformed Y'_t following Kennedy et al. (2019a), capping values above 126.0 (the 99.5
percentile of global values):

$$H_{nl} = (\log_{10} (1 + Y'_t) / 2.104) * p(C_{nl}) * I_{nl} \cdot \quad (21)$$

2.2.8 Logging

335 To estimate stressors on forested lands, we used maps of forest loss (Curtis et al. 2018) associated
with commodity-driven deforestation, shifting agriculture, and forestry. (Note that we excluded
wildfire as a stressor because of the challenges of attributing wildfires to human causation–
especially over global extent, and urbanization because it is measured directly by the built-up
stressor). We then identified locations where forest was lost due to one of the three mapped
340 stressors (using v1.6, updated to 2018; Hansen et al. 2013) prior to the year of our estimated human
modification map, and applied the intensity value associated with that stressor (Table 2). Thus,

$$H_{fr} = F_{fr} * p(C_{fr}) * I_{fr} \cdot \quad (22)$$

where F_{fr} is pixels of forested loss in a given year, and I_{fr} is an estimate of intensity associated with
the cause of forest loss.

345

2.2.9 Human intrusion

We estimated human intrusion (H_i) using a method that builds on and extends accessibility modeling
(Nelson 2008; Theobald 2008, 2013; Theobald et al. 2010; Weiss et al. 2018; Nelson et al. 2019). Human
intrusion (aka “use”: Theobald 2008) uses central place theory (Alonso 1960) and integrates human
accessibility throughout a landscape from defined locations, typically along roads and rails as well as
350 off-road areas from urban areas (Theobald et al. 2010; Esteves et al. 2011; Theobald 2013; Larson et al.
2018).

355

Accessibility measured in travel time in minutes is calculated from each mapped settlement point j
(e.g., cities, towns, villages) from GRUMP v1.01 and GPW v4 (CIESIN 2017, 2018). This approach is
much less sensitive to arbitrary thresholds of city/town size (e.g., 50,000 residents), often used due
to computational constraints (e.g. Nelson 2008; Weiss et al. 2018). Second, to estimate “intrusion” of
people to adjacent areas from a given settlement, we estimated the number of people (using
population estimates at settlement j) at a given location (X ; ~population density: people/km²)



360 following the assumption that the human density halved with every 60 minutes traveled (Theobald
2008, 2013). The resulting intrusion map for each settlement was then summed to account for typical
overlaps of intrusion from nearby settlements. We assumed that there is a limit at very high
population densities and so we capped the maximum value of intrusion, X , at 1,000,000 then
max-normalized using a square-root transform:

$$F_i = X^{0.5} * 0.001 , \quad (23)$$

365 $H_i = F_i * p(C_i) * I_i . \quad (24)$

Note that accessibility was calculated using estimates of travel time along roads and rails, as well as
off-road through different features of the landscape, using established travel time factors (Tobler
1991) and presuming walking off-trail or via boats on freshwater or along ocean shoreline (Nelson
2008; Theobald et al. 2010; Weiss et al. 2018; Nelson et al. 2019). This included effects of international
370 borders following Weiss et al. (2018), and accessibility to lands was calculated across oceans.

2.2.10 Natural systems modification

Dams and their associated reservoirs flood natural habitat and strongly impact the natural flow
regimes of the adjacent rivers (Grill et al. 2019). We mapped the footprint of reservoirs F_r created
375 from 6,849 dams from the Global Reservoirs and Dams database (GRanD v1.3; Lehner et al. 2011;
<http://globaldamwatch.org/grand/>).

$$H_r = F_r * p(C_r) * I_r . \quad (25)$$

2.2.11 Pollution

We estimated the stress of air pollution by using data on nitrogen oxides (NO_x) through time from
380 the Emissions Database for Global Atmospheric Research (EDGAR v4.3.2; Crippa et al. 2018). We
selected NO_x because it is a strong contributor to acid rain/fog and tropospheric ozone and because
atmospheric levels are predominantly from human-sources (Delmas et al. 1997). We used the 99th
percentile (46,750 M tonnes) as the maximum value and then max-normalized (F_{nox}) and adjusted
using the intensity value I_{nox} :

385 $H_{nox} = F_{nox} * p(C_{nox}) * I_{nox} . \quad (26)$

2.3 Uncertainty and validation analyses

To understand the uncertainty of our results associated with our estimated intensity values (Table 2),
following Kennedy et al. (2019b), we re-calculated H where I_s was randomized between the minimum
and maximum intensity values (at 1 km² resolution for computational efficiency). We quantified the
390 mean and standard deviation of the resulting global H values for n=50 randomizations.

We also assessed the accuracy of our maps following validation procedures described in Kennedy et
al. (2019a, 2019b, 2019c). Because historical “ground truth” human modification data in comparable
form are not widely available, we restricted our analysis to test the contemporary (~2017) conditions
395 map of human modification that included all stressor layers. We used the validation data from
Kennedy et al. (2019a), which is an independent validation dataset that quantified the degree of



human modification from visual interpretation of high resolution aerial or satellite imagery across the world. We selected plots using the Global Grid sampling design (Theobald 2016), a spatially-balanced and probability-based random sampling that was stratified on a five-class rural to urban gradient
400 using “stable nighttime-lights” 2013 imagery (Elvidge *et al.*, 2001). Within each of 1,000 ~1 km² plots, we selected 10 simple-random locations to capture rare features and heterogeneity in land use and land cover (for a total of 10,000 sub-plots), which were separated by a minimum distance of 100 m. The spatial-balanced nature of the design maximizes statistical information extracted from each plot because it increases the number of samples in relatively rare areas that are likely of interest (in
405 contrast to simple random sampling) -- especially for urbanized and growing cities (Theobald, 2016).

2.4 Processing platform

We processed, modeled, and analyzed the spatial data using the Google Earth Engine platform (Gorelick *et al.* 2017). We calculated all distances and areas using geodesic algorithms in decimal degrees (EPSG: 4326). We summarized areas and percentages after projecting the data to Mollweide
410 equal-area (WGS84) to simplify calculations. All datasets and maps conform to the Google Earth Engine terms of service. We used program R 3.6.1 (R Core Team 2019) to generate Fig. 2.

3 Results

Below we describe the temporal and spatial trends of human modification by continents (Table 4),
415 biomes (Table 5), and ecoregions (Fig. 2).

3.1 Changes from 1990-2015

The mean value of H for global terrestrial lands increased from 0.08221 in 1990 to 0.09458 in 2015, a percentage change of 15.04% (0.60% annually; Table 4). This equates to 1.6 M km² of natural lands lost -- roughly 177 km² daily or 17 football pitches per minute (i.e. an international football field). Increases
420 in human modification occurred across the globe and across urban and rural locations. We found that the largest increases in H_{mad} occurred in Oceania, followed by Asia and Europe. Australia had the lowest increase followed by North and South America (Table 4). The biomes that exhibited the greatest increases were mangroves; tropical & subtropical moist broadleaf forests; and tropical & subtropical dry broadleaf forests; while the biomes with the smallest increases were tundra; boreal forests/taiga; and deserts and xeric shrublands. Maps of changes in H_{mad} between 2015 and 1990 for each ecoregion are shown in Fig. 1a, relative to HF (Fig. 1b) and THPI (Fig. 1c). Figure 2 shows the ratio of natural land loss between 1990 and 2015, for each ecoregion and grouped by biome, in the
425 context of the contemporary extent of human modification. We found most ecoregions ($n=814$) had increased in human modification, while the few ($n=32$) that had decreased were concentrated in higher latitudes and in more remote areas. We also found that changes in H_{mad} have increased over
430 time, from 0.00042 to 0.00051 to 0.00062, during 1990-2000 to 2000-2010 to 2010-2015. The percent change has also increased over time from 0.51% to 0.59% to 0.68%.



3.2 Contemporary extent

We found that about 19.1 M km² of natural lands were lost by ~2017 – about 14.6% of land globally (Table 4). South America was the most transformed (28.7%), followed by North America (16.8%), while Australia (5.0%) and Africa (10.7%) were the least transformed. Broad-scale patterns of the extent of human modification in ~2017 are shown in Fig. 3.

Terrestrial lands with very low levels of human modification ($H < 0.01$) are concentrated in less productive and more remote areas in high latitudes and dominated by inaccessible permanent rock and ice or within tundra, boreal forests, and to a lesser extent montane grasslands. Table 5 shows that the biomes with the highest levels of H in ~2017 were temperate broadleaf and mixed forests ($H=0.37435$); tropical & subtropical dry broadleaf forests ($H=0.33170$); and Mediterranean forests, woodlands & scrub ($H=0.29027$). The five least modified biomes were tundra (mean $H=0.00230$); boreal forests/taiga ($H=0.02129$); deserts and xeric shrublands ($H=0.05706$); and montane grasslands and shrublands ($H=0.08943$).

We found that in ~2017, 51.0% of lands had very low human modification (mean $H \leq 0.01$; 66.8 M km²), 13.3% had low human modification ($0.01 < H \leq 0.1$; 17.4 M km²), 21.0% had moderate human modification ($0.1 < H \leq 0.4$; 27.6 M km²), 12.3% had high human modification ($0.4 < H \leq 0.7$; 16.1 M km²), and 2.4% had very high human modification ($0.7 < H \leq 1.0$; 3.2 M km²) (following the thresholds from Kennedy et al. 2019a). We found that ~4.2% of lands have no evidence of human modification ($H < 0.00001$; 5.5 M km²), based on our estimate of the level of precision (~0.00001) given the data inputs.

3.3 Comparisons

We compared our work to earlier efforts to determine if overall trends and extents were generally consistent and resulting priorities of biomes and ecoregions were similar. Globally, H_{mad} from 1990-2015 ($t=1990$, $u=2015$) was 0.00049, while for HF and THPI it was higher ($HF_{mad}=0.00056$, $THPI_{mad}=0.00081$). Perhaps more important is that the variability of the mean annualized difference values in the HF and THPI was 2.3 and 3.2 times that of H . By continent, we found that H_{mad} increased the most in Oceania, followed by Asia, Europe, Africa, South America, North America, and Australia. Continental ranks by THPI followed H roughly, though HF differed more substantially (Table 5). H_{mad} increased for all continents, but HF_{mad} showed declines in modification for Europe and South America, while $THPI_{mad}$ showed a decline for North America.

We also found the ranking of biomes by mean annualized difference for HF and THPI were fairly different from ranks developed from H values (Table 6). Of the three biomes with the largest increase for H_{mad} , two of them were also identified by HF (tropical & subtropical dry broadleaf forests and tropical & subtropical moist broadleaf forests) and none of them by THPI. Of the five biomes with the largest increase for H_{mad} , three of them were also identified by HF and THPI. The biomes that had the greatest disagreement amongst the ranking of H , HF, and THPI were mangroves; tropical & subtropical coniferous forests; and tropical & subtropical dry broadleaf forests. The results for



ecoregions shown in Fig. 1 are even more striking, as the mean annualized difference values for HF and THPI were inconsistent with our results. Of the 814 ecoregions that had increases in H_{mad} , a decrease in modification was found for 201 ecoregions in HF_{mad} and 202 for $THPI_{mad}$; and for the 32 ecoregions that were found to have decreases in H_{mad} , an increase in modification was found for 20 in HF and 22 in THPI.

In terms of the overall amount of recent (~2017) human modification globally, we found that 14.5% of terrestrial lands globally have been modified – which is roughly similar to HF (12.3% for ~2009; Venter et al. 2016) and the degree of human modification at 1-km resolution (H1k; 19% for ~2016; Kennedy et al. 2018, 2019a). The ranks of the extent of modification by biomes, however, were very similar between H, H1k, and HF. In general, H had intermediate modification levels compared to H1k and HF: with H1k levels being slightly higher (difference between 0.00 min to 0.09 and average difference of 0.05 by biome) and HF being slightly lower (difference between 0.00 min to 0.13 max and average difference of 0.04 by biome) (Table 6). The global estimate for H1k was likely higher than H because H1k did not limit the livestock stressor at $LU\ km^{-2} < 1.0$, used a slightly higher value for the low-threshold on the electrical infrastructure and energy use stressor (i.e. “nightlights”), and reported results that incorporate uncertainty in estimates of intensity. The biggest differences in rankings between the H and the HF were for temperate and broadleaf mixed forests (and see comparisons of H1k and HF in Kennedy et al. 2019a, 2019b).

3.4 Uncertainty and validation analyses

To examine the uncertainty associated with our intensity estimates, we calculated across all terrestrial lands the mean H value on datasets generated with intensity values drawn from a uniform random distribution between the minimum and maximum estimates. We generated 50 randomized datasets and found the mean of the randomized maps was 0.14306 and the standard deviation was ± 0.00106 (compared to our best-estimate of 0.14605). The lowest possible mean H value calculated with the minimum estimate for all stressors was 0.10686 and the highest possible value using the maximum estimate was 0.18493.

We found strong agreement between H for ~2017 and our validation data ($r=0.783$), with an average root-mean-square-error of 0.22 and a mean-absolute-error of 0.04, for the 926 ~1 km² plots (9,260 sub-plots). There were 726 plots within $\pm 20\%$ agreement, while for 161 plots H was estimated higher than our visual estimate from the validation data (and 39 plots lower). Estimates of H were biased high, likely because the stressors for the “human intrusion” and electrical infrastructure (based on nighttime lights) are not readily observable from the aerial imagery used to generate the validation data.



4 Discussion

4.1 Summary

510 We found rapid and increasing human modification of terrestrial systems, resulting in the loss of
natural lands globally. Our findings foreshadow trends and patterns of increased human
modification, assuming future trends in the next 25-30 years continue as they have recently. Thus,
our study reinforces calls for stronger commitments to help reduce habitat loss and fragmentation
(Kennedy et al. 2019a, Jacobson et al. 2019) -- which should be considered in conjunction with current
commitments (e.g., to reduce CO₂ emissions through the Paris climate accord; Baruch-Mordo et al.
515 2019; Kiesecker et al. 2019). We believe that the comparisons of ecoregions and biomes shown in Fig.
2 offer valuable contextual information that provides initial guidance on conservation strategies that
may be most appropriate (Kennedy et al. 2019a). Also, it is important to consider the relative
importance of each ecoregion towards meeting representation goals by ecoregion (Dinerstein et al.
2017) or ecosystem (Jantke et al. 2019), as well as considering additional stresses caused by climate
520 change (Costanza and Terando 2019). We emphasize that although global, continental, biome, and
ecoregional summaries provide a general idea of trends and patterns, our work here supports robust
estimates at country and within ecoregional patterns of the gradient of human modification,
especially when placed within a broader structured decision making framework (Tullock et al. 2015)

525 Our datasets of human modification provide the most granular, contemporary, comprehensive,
high-quality, and robust data currently available to assess temporal and spatial trends of global
human modification. Our work is grounded in a structured classification of stressors, uses an
internally-consistent model, evaluates uncertainty, and incorporates refinements to minimize the
effects of scaling and classification errors. Our validation approach uses an independent and
530 spatially-balanced random sample design to provide strong support for the quality of our findings
(Kennedy et al. 2019c).

Our overarching goal in producing and publishing these datasets is to support detailed quantification
of the rates and trends, as well as the current extent and pattern, to understand the gradient of the
535 degree of human modification across the continuum from low (e.g., wilderness) to high (e.g., intense
urban). Beyond the basic findings presented here, we believe there are many potential applications
of these datasets, including: examining temporal rates and trends of land modification in and around
protected areas (e.g., Geldmann et al. 2019a); estimating fragmentation for all ecoregions and
biomes (Kennedy et al. 2019a, Jacobson et al. 2019); and evaluating conservation opportunities and
540 risks (e.g., the conservation risk index; Hoekstra et al. 2005). We also note that the human
modification approach allows, in a straightforward and logically consistent way, inclusion of
additional stressors and higher resolution datasets that may become available over time or may be
available for specific, local areas.



4.2 Caveats

545 As with any model, we recognize there are limitations of our work. We did not include data for all
human stressors, typically because of incomplete global coverage or too-coarse mapping units (Klein
Goldewijk et al. 2007; Geldmann *et al.*, 2014), an inability to discern human-induced versus natural
disturbances (e.g.; wildfires), or uncertainty in the location and directionality of its impact (e.g.;
550 climate change on terrestrial systems; Geldmann *et al.*, 2014). Although our datasets described here
have order-of-magnitude higher resolution than previous temporal maps, estimates of H generated
for areas less than roughly 100 km² should be used with caution. Stressors that are particularly
important to improve include effects of grazing (currently coarse data and very broad expanse),
pasture land, invasive species, and climate change (especially effects of sea-level rise), and we
encourage future work to focus on developing appropriate datasets and approaches to include or
555 better capture these stressors. Key datasets we believe should be improved include transportation
networks (e.g., Van Etten 2019) that are comparable through time; livestock grazing, rangelands,
croplands, and pasturelands and their intensity of use; resource extraction (especially mining
footprints); and temporal trends in gas flares, utility-scale solar plants, electrical substations, etc.

4.3 Data availability

560 The datasets generated from this work are available at <https://doi.org/10.5061/dryad.n5tb2rbs1>
(Theobald et al. 2020). All other datasets used in our work are open-source data cited within.

Author contributions

DT, CK, BC, JO, SBM, JK conceived the paper; DT, CK, JO, BC prepared data; DT implemented the
model; DT, CK, BC, SBM conducted summary analyses; DT, CK, BC, JO, SBM, JK developed
565 recommendations; all contributed to writing the manuscript.

Competing interests. The authors declare that they have no conflict of interest.

Acknowledgments

570 We thank OpenStreetMap contributors (copyright OpenStreetMap and data are available from
<https://www.openstreetmap.org>), and E. Lebre for assistance with the global mining data.

References

- Allred, B. W., Smith, W. K., Tidwell, D., Haggerty, J.H., Running, S. W., Naugle, D.E., Fuhlendorf, S.D.:
Ecosystem services lost to oil and gas in North America. *Science*, 348(6233):401-402, 2015.
Alonso, W.: A theory of the urban land market. *Papers in Regional Science*, 6(1), 149-157, 1960.



- 575 van Asselen, S., Verburg, P. H.: A Land System representation for global assessments and land-use modeling. *Global Change Biology*, 18(10), 3125-3148, 2012.
- Baruch-Mordo, S., Kiesecker, J., Kennedy, C.M., Oakleaf, J.R. and Opperman, J.J.: From Paris to practice: sustainable implementation of renewable energy goals. *Environmental Research Letters*. <https://iopscience.iop.org/article/10.1088/1748-9326/aaf6e0>, 2019.
- 580 Bonham-Carter, G.F.: *Geographic information systems for geoscientists: modelling with GIS (Vol. 13)*, Elsevier, 2014.
- Brown, M. T., Vivas, M. B.: Landscape development intensity index. *Environmental Monitoring and Assessment*, 101(1-3), 289-309, 2005.
- Center for International Earth Science Information Network - CIESIN - Columbia University, CUNY
585 Institute for Demographic Research - CIDR, International Food Policy Research Institute - IFPRI, The World Bank, and Centro Internacional de Agricultura Tropical - CIAT.: *Global Rural-Urban Mapping Project, Version 1 (GRUMPv1): Settlement Points, Revision 01*. Palisades, NY: NASA Socioeconomic Data and Applications Center (SEDAC). <https://doi.org/10.7927/H4BC3WG1>, 2017, Accessed 1 January 2019.
- 590 Center for International Earth Science Information Network - CIESIN - Columbia University. *Gridded Population of the World, Version 4 (GPWv4): Administrative Unit Center Points with Population Estimates, Revision 11*. Palisades, NY: NASA Socioeconomic Data and Applications Center (SEDAC). <https://doi.org/10.7927/H4BC3WMT>, 2018, Accessed 1 January 2019.
- Chaudhary, A. Brooks, T.M.: Land use intensity-specific global characterization factors to assess
595 product biodiversity footprints. *Environmental Science & Technology*, 52(9), 5094-5104, 2018.
- Corbane, C., Florczyk, A., Pesaresi, M., Politis, P., Syrris, V.: GHS built-up grid, derived from Landsat, multitemporal (1975-1990-2000-2014), R2018A. European Commission, Joint Research Centre (JRC) doi: [10.2905/jrc-ghsl-10007](https://doi.org/10.2905/jrc-ghsl-10007) PID: <http://data.europa.eu/89h/jrc-ghsl-10007>, 2018
- Costanza, J.K., Terando, A.J.: Landscape Connectivity Planning for Adaptation to Future Climate and
600 Land-Use Change. *Current Landscape Ecology Reports*, 4(1), pp.1-13, 2019.
- Crippa, M., Guizzardi, D., Muntean, M., Schaaf, E., Dentener, F., van Aardenne, J. A., Janssens-Maenhout, G.: Gridded emissions of air pollutants for the period 1970–2012 within EDGAR v4. 3.2. *Earth System Science Data*, 10(4), 1987-2013, 2018.
- Curtis, P.G., Slay, C.M., Harris, N.L., Tyukavina, A., Hansen, M.C.: Classifying drivers of global forest
605 loss. *Science*, 361(6407), pp.1108-1111, <https://science.sciencemag.org/content/sci/suppl/2018/09/12/361.6407.1108.DC1>, 2018.
- Delmas, R., Serca, D., Jambert, C.: Global inventory of NO_x sources. *Nutrient cycling in Agroecosystems*, 48(1-2), 51-60, 1997.
- Demographia. *Demographia World Urban Areas 12th Annual Edition*. pp 110,
610 <http://www.demographia.com/db-worldua.pdf>, 2016.
- Dinerstein, E., Olson, D., Joshi, A., Vynne, C., Burgess, N.D., Wikramanayake, E., Hahn, N., Palminteri, S., Hedao, P., Noss, R., Hansen, M.: An ecoregion-based approach to protecting half the terrestrial realm. *BioScience*, 67(6), 534-545, 2017.
- Dinerstein, E., Vynne, C., Sala, E., Joshi, A. R., Fernando, S., Lovejoy, T. E., Burgess, N. D.: A Global Deal
615 For Nature: Guiding principles, milestones, and targets. *Science Advances*, 5(4), eaaw2869, 2019.



- Ellis, E. C., Ramankutty, N.: Putting people in the map: anthropogenic biomes of the world. *Frontiers in Ecology and the Environment*, 6,8: 439-447, 2008.
- 620 Elvidge, C.D., Imhoff, M.L., Baugh, K.E.: Night-time lights of the world: 1994–1995. *ISPRS Journal of Photogrammetry and Remote Sensing*, 56, 81-99, 2001.
- Elvidge, C., Ziskin, D., Baugh, K., Tuttle, B., Ghosh, T., Pack, D., Erwin, E., Zhizhin, M.: A Fifteen Year Record of Global Natural Gas Flaring Derived from Satellite Data. *Energies* 2 (3): 595, doi:10.3390/en20300595, 2009.
- 625 Elvidge, C. D., Baugh, K. E., Zhizhin, M., Hsu, F. C.: Why VIIRS data are superior to DMSP for mapping nighttime lights. *Proceedings of the Asia-Pacific Advanced Network*, 35(0), 62, 2013.
- Elvidge, C., Zhizhin, M., Baugh, K., Hsu, F. C., & Ghosh, T.: Methods for global survey of natural gas flaring from visible infrared imaging radiometer suite data. *Energies*, 9(1), 14, 2016.
- ESA CCI. Land Cover CCI Product User Guide v2 (CCI-LC-PUGv2). Table 3-6, 2017.
- 630 Esteves, C.F., de Barros Ferraz, S.F., de Barros, K.M., Ferraz, M.G., Theobald, D.M.: Human accessibility modelling applied to protected areas management. *Natureza & Conservacao*, 9(2):232-9, 2011.
- van Etten, A.: City-scale road extraction from satellite imagery. arXiv:1904.09901v2 [cs.CV] 22 Jul 2019.
- 635 Fritz, S., See, L., Perger, C., McCallum, I., Schill, C., Schepaschenko, D., Lesiv, M.: A global dataset of crowdsourced land cover and land use reference data. *Scientific Data*, 4, 170075, 2017.
- Gardner, R. H., Urban, D. L.: Neutral models for testing landscape hypotheses. *Landscape Ecology*, 22(1), 15-29, 2007.
- Geldmann, J., Joppa, L. N., Burgess, N.D.: Mapping change in human pressure globally on land and within protected areas. *Conservation Biology*, 28(6), 1604-1616, 2014.
- 640 Geldmann, J., Manica, A., Burgess, N.D., Coad, L., Balmford, A.: A global-level assessment of the effectiveness of protected areas at resisting anthropogenic pressures. *Proceedings of the National Academy of Sciences*, 116(46), 23209-23215, 2019a.
- Geldmann, J., Joppa, L., Burgess, N.D.: Temporal Human Pressure Index, v2, Dryad, Dataset, <https://doi.org/10.5061/dryad.p8cz8w9kf>, 2019b.
- 645 Gerber, P., Mooney, H.A., Dijkman, J., Tarawal, S., De Haan, C.: *Livestock in a Changing Landscape, Volume 2: Experiences and Regional Perspectives*, Washington, D.C., Island Press, 2010.
- Gilbert, M., Nicolas, G., Cinardi, G., Van Boeckel, T. P., Vanwambeke, S. O., Wint, G. W., Robinson, T. P.: Global distribution data for cattle, buffaloes, horses, sheep, goats, pigs, chickens and ducks in 2010. *Scientific Data*, 5, 180227, 2018a.
- 650 Gilbert, M., Nicolas, G., Cinardi, G., Van Boeckel, T. P., Vanwambeke, S. O., Wint, G. W., Robinson, T. P. Global distribution data for cattle, buffaloes, horses, sheep, goats, pigs, chickens and ducks in 2010. *Scientific Data*, 5, 180227, <https://doi.org/10.7910/DVN/BLWPZN>, <https://doi.org/10.7910/DVN/33NoJG>, <https://doi.org/10.7910/DVN/7Q52MV>, <https://doi.org/10.7910/DVN/OCPH42>, <https://doi.org/10.7910/DVN/ICHCBH>, <https://doi.org/10.7910/DVN/GIVQ75>, <https://doi.org/10.7910/DVN/SUFASB>, <https://doi.org/10.7910/DVN/5U8MWJ>, 2018b.
- 655 González-Abraham, C., Ezcurra, E., Garcillán, P. P., Ortega-Rubio, A., Kolb, M., Creel, J. E. B.: The human footprint in Mexico: physical geography and historical legacies. *PloS ONE*, 10(3), e0121203, 2015.



- 660 Gorelick, N., Hancher, M., Dixon, M., Ilyushchenko, S., Thau, D., Moore, R. Google Earth Engine: Planetary-scale geospatial analysis for everyone. *Remote Sensing of Environment*, 202, pp. 18-27, 2017.
- Grill, G., Lehner, B., Thieme, M., Geenen, B., Tickner, D., Antonelli, F., Macedo, H. E.: Mapping the world's free-flowing rivers. *Nature*, 569(7755), 215, 2019.
- 665 Haddad, N. M., Brudvig, L. A., Clobert, J., Davies, K. F., Gonzalez, A., Holt, R. D., Cook, W. M.: Habitat fragmentation and its lasting impact on Earth's ecosystems. *Science Advances*, 1(2), e1500052, 2015.
- Hajkovicz, S., Collins, K.: A review of multiple criteria analysis for water resource planning and management. *Water Resources Management*, 21(9), pp.1553-1566, 2007.
- 670 Halpern, B.S., Mcleod, K.L, Rosenberg, A.A., Crowder, L.B.: Managing for cumulative impacts in ecosystem-based management through ocean zoning. *Ocean & Coastal Management* 51, 203-211, 2008.
- Halpern, B.S., Fujita, R.: Assumptions, challenges, and future directions in cumulative impact analysis. *Ecosphere*, 4, 1-11, 2013.
- 675 Hansen, M. C., Potapov, P. V., Moore, R., Hancher, M., Turubanova, S. A. A., Tyukavina, A., Kommareddy, A.: High-resolution global maps of 21st-century forest cover change. *Science*, 342(6160), 850-853, 2013.
- Hoekstra, J.M., Boucher, T.M., Ricketts, T.H., Roberts, C.: Confronting a biome crisis: global disparities of habitat loss and protection. *Ecology Letters*, 8(1), pp.23-29, 2005.
- 680 IPBES. Summary for policymakers of the global assessment report on biodiversity and ecosystem services of the Intergovernmental Science-Policy Platform on Biodiversity and Ecosystem Services. S. Díaz, J. Settele, E. S. Brondizio E.S., H. T. Ngo, M. Guèze, J. Agard, A. Arneth, P. Balvanera, K. A. Brauman, S. H. M. Butchart, K. M. A. Chan, L. A. Garibaldi, K. Ichii, J. Liu, S. M. Subramanian, G. F. Midgley, P. Miloslavich, Z. Molnár, D. Obura, A. Pfaff, S. Polasky, A. Purvis, J. Razzaque, B. Reyers, R. Roy Chowdhury, Y. J. Shin, I. J. Visseren-Hamakers, K. J. Willis, and C. N. Zayas (eds.). IPBES secretariat, Bonn, Germany, 2019.
- IPCC: Climate change and land: summary for policymakers. URL: <https://www.ipcc.ch/report/srccl/>, 2019. Accessed November 21, 2019.
- 690 Jacobson, A.P., Riggio, J., Tait, A., Baillie, J.: Global areas of low human impact ('Low Impact Areas') and fragmentation of the natural world. *Scientific Reports*, 2019.
- Jantke, K., Kuempel, C.D., McGowan, J., Chauvenet, A.L., Possingham, H.P.: Metrics for evaluating representation target achievement in protected area networks. *Diversity and Distributions*, 25(2), pp.170-175, 2019.
- 695 Jordan, M., Meyer, W. B., Kates, R. W., Clark, W. C., Richards, J. F., Turner, B. L., Mathews, J. T.: *The earth as transformed by human action: global and regional changes in the biosphere over the past 300 years*. CUP Archive, 1990.
- Kehoe, L., Romero-Muñoz, A., Polaina, E., Estes, L., Kreft, H., Kuemmerle, T.: Biodiversity at risk under future cropland expansion and intensification. *Nature Ecology & Evolution*, 1(8), 1129, doi:[10.1038/s41559-017-0234-3](https://doi.org/10.1038/s41559-017-0234-3), 2017.
- 700 Kiesecker, J., Baruch-Mordo, S., Kennedy, C.M., Oakleaf, J.R., Baccini, A. and Griscom, B.W.: Hitting the Target but Missing the Mark: Unintended Environmental Consequences of the Paris



- Climate Agreement. *Frontiers in Environmental Science*,
<https://doi.org/10.3389/fenvs.2019.00151>, 2019.
- 705 Kennedy, C.M., Oakleaf, J.R., Theobald, D.M., Baruch-Mordo, S., Kiesecker, J.: Managing the middle:
A shift in conservation priorities based on the global human modification gradient. *Global
Change Biology*, 25(3), 811-826, 2019a.
- Kennedy, C.M., Oakleaf, J.R., Theobald, D.M., Baruch-Mordo, S., Kiesecker, J.: Supplementary
information for: Managing the middle: A shift in conservation priorities based on the global
710 human modification gradient. *Global Change Biology*, 25(3), 811-826, 2019b.
- Kennedy, C.M., Oakleaf, J.R., Baruch-Mordo, S., Theobald, D.M. & Kiesecker, J.: Finding middle
ground: Extending conservation beyond wilderness areas. *Global Change Biology*
doi:10.1111/gcb.14900, 2019c.
- Kennedy, C.M., Oakleaf, J., Theobald, D.M., Baruch-Mordo, S., Kiesecker, J.: Global Human
715 Modification. figshare. Dataset. <https://doi.org/10.6084/m9.figshare.7283087.v1>, 2018.
- Klein Goldewijk, K., Van Drecht, G. and Bouwman, A.F.: Mapping contemporary global cropland and
grassland distributions on a 5×5 minute resolution. *Journal of Land Use Science*, 2(3),167-190,
2007.
- Larson, C.L., Reed, S.E., Merenlender, A.M., Crooks, K.R.: Accessibility drives species exposure to
720 recreation in a fragmented urban reserve network. *Landscape and Urban Planning* 175:62-71,
2018.
- Lehner, B., Liermann, C. R., Revenga, C., Vörösmarty, C., Fekete, B., Crouzet, P., Nilsson, C.:
High-resolution mapping of the world's reservoirs and dams for sustainable river-flow
management. *Frontiers in Ecology and the Environment*, 9(9), 494-502, 2011.
- 725 Li, X., Zhou, Y.: Urban mapping using DMSP/OLS stable night-time light: a review, *International
Journal of Remote Sensing*, 38:21, 6030-6046, DOI: 10.1080/01431161.2016.1274451, 2017.
- Li, W., MacBean, N., Ciais, P., Defourny, P., Lamarche, C., Bontemps, S., Houghton, R. A., and Peng, S.:
Gross and net land cover changes in the main plant functional types derived from the annual
ESA CCI land cover maps (1992–2015), *Earth Syst. Sci. Data*, 10, 219-234,
730 <https://doi.org/10.5194/essd-10-219-2018>, 2018.
- McBride, M. F., Garnett, S. T., Szabo, J. K., Burbidge, A. H., Butchart, S. H., Christidis, L., Burgman,
M.A.: Structured elicitation of expert judgments for threatened species assessment: a case
study on a continental scale using email. *Methods in Ecology and Evolution*, 3(5), 906-920,
2012.
- 735 Malczewski, J.: GIS and multicriteria decision analysis. John Wiley & Sons, 1999.
- Marsh, G. P.: *The earth as modified by human action*, C. Scribner's Sons, 1885.
- Nelson, A.: Travel time to major cities: a global map of accessibility. Report to: Global Environment
Monitoring Unit, Joint Research Centre of the European Commission, 2008.
- Nelson, A., Weiss, D.J., van Etten, J., Cattaneo, A., McMenomy, T.S., Koo, J.: A suite of global
740 accessibility indicators. *Scientific Data*, 6(1), pp.1-9, 2019.
- OpenStreetmap, www.openstreetmap.org. 2019. Accessed April 27, 2019.
- Pekel, J. F., Cottam, A., Gorelick, N., Belward, A. S.: High-resolution mapping of global surface water
and its long-term changes. *Nature*, 540(7633), 418, 2016.
- Pérez-Hoyos, A., Rembold, F., Kerdiles, H. and Gallego, J.: Comparison of global land cover datasets
745 for cropland monitoring. *Remote Sensing*, 9(11), p.1118, 2017.



- Pesaresi, M., Ehrlich, D., Florczyk, A.J., Freire, S., Julea, A., Kemper, T., Soille, P. and Syrris, V. GHS built-up grid, derived from Landsat, multitemporal (1975, 1990, 2000, 2015). European Commission, Joint Research Centre, JRC Data Catalogue, 2015.
- 750 R Core Team: R: A language and environment for statistical computing. R Foundation for Statistical Computing, Vienna, Austria. <https://www.R-project.org/>, 2019.
- Riitters, K.H., Wickham, J.D. and Wade, T.G.: An indicator of forest dynamics using a shifting landscape mosaic. *Ecological Indicators*, 9(1), pp.107-117, 2009.
- Robinson, T. P., Wint, G. W., Conchedda, G., Van Boeckel, T. P., Ercoli, V., Palamara, E., Gilbert, M.: Mapping the global distribution of livestock. *PloS one*, 9(5), e96084, 2014.
- 755 Roszkowska, E.: Rank ordering criteria weighting methods—a comparative overview. *OPTIMUM. STUDIA EKONOMICZNE NR 5 (65): 14-33*, 2013.
- S&P. S&P Global Market Intelligence. Thomson Reuters, New York, United States, 2018.
- Salafsky, N., Salzer, D., Stattersfield, A. J., Hilton-Taylor, C., Neugarten, R., Butchart, S. H., Wilkie, D.: A standard lexicon for biodiversity conservation: unified classifications of threats and actions. 760 *Conservation Biology*, 22(4), 897-911, 2008.
- Sanderson, E. W., Jaiteh, M., Levy, M. A., Redford, K. H., Wannebo, A. V., Woolmer, G.: The human footprint and the last of the wild. *BioScience*, 52(10), 891-904, 2002.
- Schultz, M.T.: A critique of EPA's index of watershed indicators. *Journal of Environmental Management*, 62(4), pp.429-442, 2001.
- 765 Secretariat of the Convention on Biological Diversity.: Strategic plan for biodiversity 2011–2020 and the Aichi targets, 2010. URL: <https://www.cbd.int/sp/targets/default.shtml> (Accessed 24 December 2018).
- Speirs-Bridge, A., Fidler, F., McBride, M., Flander, L., Cumming, G., Burgman, M.: Reducing overconfidence in the interval judgments of experts. *Risk Analysis: An International Journal*, 770 30(3), 512-523, 2010.
- Theobald, D.M.: Reducing linear and perimeter measurement errors in raster-based data. *Cartography and Geographic Information Science* 27(2), 111-116, 2000.
- Theobald D.M.: Network and accessibility methods to estimate the human use of ecosystems. In: Proceedings of the 11th AGILE international conference on geographic information science. 775 University of Girona, Spain, 2008.
- Theobald, D.M.: Estimating natural landscape changes from 1992 to 2030 in the conterminous US. *Landscape Ecology*, 25(7), 999-1011, 2010.
- Theobald, D.M, Norman, J.B., Newman, P.: Estimating visitor use of protected areas by modeling accessibility: A case study in Rocky Mountain National Park, Colorado. *Journal of* 780 *Conservation Planning*, 6:1-20, 2010.
- Theobald, D.M.: A general model to quantify ecological integrity for landscape assessments and US application. *Landscape Ecology*, 28(10), 1859-1874, 2013.
- Theobald, D.M.: A general-purpose spatial survey design for collaborative science and monitoring of global environmental change: the global grid. *Remote Sensing*, 8(10), p.813, 2016.
- 785 Theobald, D.M., Kennedy, C., Chen, B., Oakleaf, J., Baruch-Mordo, S., Kiesecker, J.: Data for detailed temporal mapping of global human modification from 1990 to 2017, v4, Dryad, Dataset, <https://doi.org/10.5061/dryad.n5tb2rbs1>, 2020.



- 790 Titeux, N., Henle, K., Mihoub, J. B., Regos, A., Geijzendorffer, I. R., Cramer, W., Verburg, P.H., Brotons,
L.: Biodiversity scenarios neglect future land-use changes. *Global Change Biology*, 22(7),
2505-2515, 2016.
- Tobler, W.: Non-isotropic geographic modeling. National Center for Geographic Information and
Analysis Technical Report TR-93-1, 1991.
- 795 Tulloch, V. J., Tulloch, A. I., Visconti, P., Halpern, B. S., Watson, J. E., Evans, M. C., Giakoumi, S.: Why
do we map threats? Linking threat mapping with actions to make better conservation
decisions. *Frontiers in Ecology and the Environment*, 13(2), 91-99, 2015.
- UNEP-WCMC and IUCN, Protected Planet: The World Database on Protected Areas (WDPA), February
2019, Cambridge, UK: UNEP-WCMC and IUCN, 2019.
- 800 Valenta, R. K., Kemp, D., Owen, J. R., Corder, G. D., Lèbre, É.: Re-thinking complex orebodies:
Consequences for the future world supply of copper. *Journal of Cleaner Production*, 220,
816-826, 2019.
- Venter, O., Sanderson, E.W., Magrath, A., Allan, J.R., Beher, J., Jones, K.R., Possingham, H.P.,
Laurance, W.F., Wood, P., Fekete, B.M., Levy, M.A., Watson, J.E.M.: [Global terrestrial Human
Footprint maps for 1993 and 2009. *Sci. Data* 3:160067. DOI: 10.1038/sdata.2016.67](#), 2016.
- 805 Verdone, M., Seidl, A.: Time, space, place, and the Bonn Challenge global forest restoration target.
Restoration Ecology, 25, 903-911, 2017.
- Vitousek, P. M., Mooney, H. A., Lubchenco, J., Melillo, J. M.: Human domination of Earth's
ecosystems. *Science*, 277(5325), 494-499, 1997.
- Waldner, F., Fritz, S., Di Gregorio, A., Plotnikov, D., Bartalev, S., Kussul, N., Löw, F.: A unified cropland
layer at 250 m for global agriculture monitoring. *Data*, 1(1), 3, 2016.
- 810 Weiss, D.J., Nelson, A., Gibson, H.S., Temperley, W., Peedell, S., Lieber, A., Hancher, M., Poyart, E.,
Belchior, S., Fullman, N., Mappin, B.: A global map of travel time to cities to assess
inequalities in accessibility in 2015. *Nature*. 553(7688):333, 2015.
- Wickham, J., Stehman, S. V., Gass, L., Dewitz, J. A., Sorenson, D. G., Granneman, B. J., Baer, L. A.:
815 Thematic accuracy assessment of the 2011 national land cover database (NLCD). *Remote
Sensing of Environment*, 191, 328-341, 2017.
- WRI. Global Energy Observatory, Google, KTH Royal Institute of Technology in Stockholm, Enipedia,
World Resources Institute. Global Power Plant Database. Published on Resource Watch and
Google Earth Engine; <http://resourcewatch.org>, 2019. Accessed 14 April 2019.
- 820 Zhang, Q., Pandey, B., Seto, K.C.: A robust method to generate a consistent time series from
DMSP/OLS nighttime light data. *IEEE Transactions on Geoscience and Remote Sensing*
54(10):5821-31, 2016.

Author information

David M. Theobald^{1,2}, Christina Kennedy³, Bin Chen⁴, James Oakleaf³, Sharon Baruch-Mordo³, Joe
Kiesecker³

825 ¹Conservation Planning Technologies, Fort Collins, CO 80521, USA

²Department of Fish, Wildlife, and Conservation Biology, Colorado State University, Fort Collins, CO
80523, USA

<https://doi.org/10.5194/essd-2019-252>
Preprint. Discussion started: 20 February 2020
© Author(s) 2020. CC BY 4.0 License.



³Global Lands Program, The Nature Conservancy, Fort Collins, CO 80524, USA

⁴Department of Land, Air and Water Resources, University of California, Davis, CA 95616, USA

830



Tables

835

Table 1. Overview of stressors, datasets, spatial resolution, and years data were available and used in the maps of human modification. Stressor classification levels in parentheses correspond to those within the Direct Threats Classification v2 (Salafsky et al. 2008). Acronyms of source data are bolded in Source column for reference throughout the paper.

Class	Stressor*	Source	Resolution (km ²)	Year(s)
Urban & built-up (1)	Built-up (1.1, 1.2)	Global Human Settlement Layer version R2018A (GHSL ; Pesaresi et al. 2015)	0.0009 - 0.9	1990, 2000, 2010*, 2015
Agriculture (2)	Croplands & pasturelands (2.1)	European Space Agency Climate Change Initiative land cover (ESA CCI ; Li et al. 2018)	0.9	1992, 2000, 2010, 2015
		Unified Cropland Layer (UCL ; Waldner et al. 2016)	1	2010
	Grazing (2.3)	Gridded Livestock of the World v3 (GLW ; Robinson et al. 2014; Gilbert et al. 2018a, Gilbert et al. 2018b)	10	2010
Energy production & mining (3)	Oil & gas production (3.1)	Nighttime flares from Defense Meteorological Program/Operational Line-scan System (DMSP/OLS , Elvidge et al. 2009) and Visible Infrared Imaging Radiometer Suite (VIIRS , Elvidge et al. 2016)	0.25 - 1.0	2016
	Mining & quarrying (3.2)	S&P global mining dataset (S&P 2018; Valenta et al. 2019)	~1:10000	1990, 2000, 2010, 2015, 2018
	Renewable (3.3) and non-renewable power (1.2) generation	World Resources Institute Power plants (WRI ; WRI 2019)	~1:100000	1990, 2000, 2010, 2015, 2018
Transportation & service	Roads (4.1)	OpenStreetMap highway, minor, and two-track features (OSM ;	~1:10-25000	2019



corridors (4)		OpenStreetMap 2019)		
	Railways (4.1)	OSM railway features (OpenStreetMap 2019)	~1:10-25000	2019
	Powerlines (4.2)	OSM power line features (OpenStreetMap 2019)	~1:10-25000	2019
	Electrical infrastructure (4.2)	Nighttime lights from DMSP/OLS and VIIRS (Elvidge et al. 2001; Doll 2008; Elvidge et al. 2013; Zhang et al. 2016)	0.25 - 1.0	1992, 2000, 2010, 2015, 2018
Biological harvesting (5)	Logging & wood harvesting (5.3)	Forest loss (Curtis et al. 2018) and forest change (Hansen et al. 2013)	0.09 - 100	2000, 2010, 2018
Human intrusions (6)	Human intrusions (1.3, 5.1, 5.2, 6.1)	Human intrusion (Theobald 2008) using accessibility and population from Global Rural-Urban Mapping Project v1.01 (GRUMP ; CIESIN 2017) and Gridded Population of the World v4 (GPW ; CIESIN 2018)	1	1990*, 2000, 2010, 2015
Natural system modifications (7)	Reservoirs (7.2)	Global Reservoirs and Dams (GRand v1.3; Lehner et al. 2011); http://globaldamwatch.org/grand/	~1:25000	1990, 2000, 2010, 2017
Pollution (9)	Air pollution (9.5)	Emissions Database for Global Atmospheric Research (EDGAR v4.3.2; Crippa et al. 2018) for nitrogen oxides	~100	1990, 2000, 2010, 2012

840

*Based on interpolation.



845

Table 2. Estimates of the intensity value for each stressor. “Best” estimates were determined from Brown and Vivas (2005)¹, Theobald (2013)², Kennedy et al. (2019a)³, or expert judgement⁴, and are bracketed by a minimum and maximum range, following the lowest-highest-best estimate elicitation procedure to reduce bias (McBride *et al.*, 2012). Results presented here use the best estimate, while minimum and maximum estimates are used to specify the range of possible randomized intensity values in the uncertainty analysis.

Class	Stressor	Minimum	Best	Maximum
Urban & built-up	Built-up areas ^{3,4}	0.69	0.85	1.00
Agriculture	Cropland/pasture ³			
	- Minimal ⁴	0.29	0.34	0.39
	- Light ⁴	0.35	0.45	0.55
	- Intense ^{1,4}	0.60	0.65	0.70
	Livestock grazing ¹	0.20	0.28	0.37
Energy production & mining	Oil & gas production ^{1,3}	0.70	0.85	1.00
	Mining ³	0.83	0.91	1.00
	Power generation ¹ (non-renewable)	0.70	0.85	1.00
	Power generation (renewable) ¹	0.70	0.80	0.90
Transportation & service corridors*	Major roads ¹	0.78 (20)	0.80 (30)	0.83 (40)
	Minor roads ¹	0.39 (15)	0.44 (20)	0.50 (25)
	Two-track roads ¹	0.10 (3)	0.15 (5)	0.20 (10)
	Railways ¹	0.78 (15)	0.80 (20)	0.83 (25)
	Powerlines ²	0.10	0.15	0.20
	Electrical infrastructure (night-time lights) ³	0.20	0.35	0.50
Biological harvesting	Logging & wood harvesting ^{1,4**}			
	- Commodity-driven ^{1,4}	0.60	0.65	0.07
	- Shifting agriculture ^{1,4}	0.10	0.20	0.30
	- Forestry ^{1,4}	0.10	0.20	0.30



Human intrusion	Human intrusion ^{3,4}	0.20	0.35	0.50
Natural systems modification	Reservoirs ⁴	0.60	0.65	0.70
Pollution	Air pollution ^{4, ****}	0.05	0.10	0.20

850 *Assumed width of roads and railways (meters) provided in parentheses. Use of roads is incorporated into estimates of human “intrusion”.

**Causes of forest loss due to wildfire was not included because of the challenges in understanding human-causation/suppression, especially over a global extent. Also, cause of loss due to urbanization was not included in this stressor because it is incorporated directly in the built-up stressor.

855 ***Minimum value is half of best, maximum is twice of best.



860

Table 3. Probability of a land cover type being classified as cropland or pasture, calculated using the producer’s accuracy, which is how often features on the ground are classified, or the probability that a certain pixel is classified as a given land cover class. Probabilities of being cropland or pasture cover type (C_{cp}) are adjusted based on patch size (A) for patches with $A < 1 \text{ km}^2$, where $p(C_{cp}) = C_{cp} * A_{cp}^2$.

Value	Name	Crop/ pastureland weight	Proability crop/pastureland
10	Cropland, rainfed	1	0.887
20	Cropland, irrigated	1	0.893
30	Mosaic cropland (>50%)	0.5	0.387
40	Mosaic cropland (>50%)	0.25	0.366
50	Tree (>15%), broadleaved, evergreen	0	0.038
60	Tree (>15%), broadleaved, deciduous	0	0.070
70	Tree (>15%), needleleaved, evergreen	0	0.016
80	Tree (>15%), neeleaved, deciduous	0	0.000
90	Tree, mixed leaf type	0	0.000
100	Mosaic tree/shrub (>50%)	0	0.345
110	Mosaic herbaceous (>50%)	0	0.091
120	Shrubland	0	0.104
130	Grassland	0	0.176
140	Lichens and mosses	0	0.000
150	Sparse vegetation (<15%)	0	0.032
160	Tree, flooded	0	0.043
170	Tree, flooded saline	0	0.000
180	Shrub/herbaceous flooded	0	0.000
190	Urban areas	0	0.120
200	Bare	0	0.011
210	Water	0	0.018
220	Permanent snow & ice	0	0.000



865

Table 4. Summary of estimates of the degree of human modification (H) and the mean annualized difference between 5- or 10-yr increments for which change over time can be calculated (1990, 2000, 2010, and 2015), and H values for the contemporary dataset (~2017, all stressors). Mean annualized mean difference is calculated as the mean value across the continents of the difference in H values divided by the number of years (e.g., $H_{mad} = [H_{2015} - H_{1990}] / 25$).

Continent	Mean H				Mean annualized difference				~2017		
	1990	2000	2010	2015	1990-2000	2000-2010	2010-2015	1990-2015	Median	Mean	Std. Dev.
Africa	0.0457	0.0489	0.0515	0.0530	0.00032	0.00026	0.00030	0.00029	0.0056	0.1073	0.1730
Asia	0.0856	0.0915	0.0988	0.1025	0.00059	0.00073	0.00075	0.00067	0.0056	0.1542	0.2286
Australia	0.0313	0.0324	0.0334	0.0341	0.00011	0.00011	0.00013	0.00011	0.0006	0.0495	0.1250
Europe	0.1145	0.1187	0.1206	0.1226	0.00042	0.00019	0.00041	0.00033	0.0136	0.1533	0.2279
No. America	0.0408	0.0419	0.0461	0.0463	0.00011	0.00042	0.00005	0.00022	0.1309	0.1680	0.1681
Oceania	0.0431	0.0475	0.0580	0.0662	0.00044	0.00105	0.00164	0.00093	0.0527	0.1592	0.1856
So. America	0.2378	0.2398	0.2434	0.2442	0.00020	0.00036	0.00015	0.00026	0.2324	0.2868	0.2717
<u>Global</u>	<u>0.0822</u>	<u>0.0864</u>	<u>0.0915</u>	<u>0.0946</u>	<u>0.00042</u>	<u>0.00051</u>	<u>0.00062</u>	<u>0.00049</u>	<u>0.0096</u>	<u>0.1461</u>	<u>0.2146</u>

870



875

Table 5. A comparison of the mean annualized difference of human modification values for changes from 1990 to 2015 (H , 1990-2015), human footprint (HF, 1993-2009; Venter et al. 2016), and the temporal human pressure index (THPI, 1995-2010, Geldmann et al. 2019). Mean annualized mean difference is calculated as the mean value of the difference in H values divided by the number of years (e.g., $H_{mad} = [H_{2015} - H_{1990}] / 25$).

Continent	H	HF	THPI
Africa	0.00029	0.00069	0.00106
Asia	0.00068	0.00085	0.00123
Australia	0.00011	0.00018	0.00012
Europe	0.00033	-0.00023	0.00024
North America	0.00022	0.00271	-0.00014
Oceania	0.00093	0.00113	0.00072
South America	0.00025	-0.00004	0.00024
<u>Global</u>	0.00050	0.00056	0.00081



880 Table 6. Summary of results by biome, comparing trends using the mean annualized difference for
 the human modification (H_{mad}), human footprint (HF_{mad} , Venter et al. 2016), and the mean temporal
 human pressure index ($THPI_{mad}$, Geldmann et al. 2019) score. Also provided are estimates of the
 proportion of terrestrial lands modified as estimated from Kennedy et al. (H1k; 2019), and HF (score
 885 was max-normalized to rescale to 0-1). The THPI dataset characterizes only change and so estimates
 of the proportion of lands modified in 2010 could not be provided. Mean annualized mean difference
 is calculated as the mean value across the continents and globally of the difference in H values
 divided by the number of years.

Biome name	H_{mad} (1990-2015)	HF_{mad} (1993-2009)	$THPI_{mad}$ (1995-2010)	H (~2017)	H1k (~2016)	HF (2009)
Boreal Forests/Taiga	0.000004	-0.000014	0.000001	0.0213	0.0374	0.0288
Deserts & Xeric Shrublands	0.000010	0.000028	0.000032	0.0571	0.1059	0.0820
Flooded Grasslands & Savannas	0.000022	0.000023	0.000152	0.2024	0.2480	0.1423
Mangroves	0.000050	0.000047	0.000021	0.2165	0.3051	0.1972
Mediterranean Forests, Woodlands & Scrub	0.000033	0.000078	0.000120	0.2903	0.3373	0.2162
Montane Grasslands & Shrublands	0.000013	0.000059	0.000057	0.0894	0.1634	0.1076
Temperate Broadleaf & Mixed Forests	0.000023	0.000027	0.000022	0.3744	0.3968	0.2485
Temperate Conifer Forests	0.000016	0.000011	0.000057	0.1072	0.1561	0.0992
Temperate Grasslands, Savannas & Shrublands	0.000015	0.000006	0.000092	0.2374	0.2943	0.1668
Tropical & Subtropical Coniferous Forests	0.000032	0.000005	0.000247	0.2052	0.2606	0.1568
Tropical & Subtropical Dry Broadleaf Forests	0.000046	0.000118	0.000056	0.3317	0.4242	0.2265
Tropical & Subtropical Grasslands, Savannas & Shrublands	0.000020	0.000057	0.000084	0.1476	0.2120	0.1207
Tropical & Subtropical Moist Broadleaf Forests	0.000047	0.000074	0.000092	0.1862	0.2310	0.1390
Tundra	0.000001	0.000001	-0.000001	0.0023	0.0001	0.0066

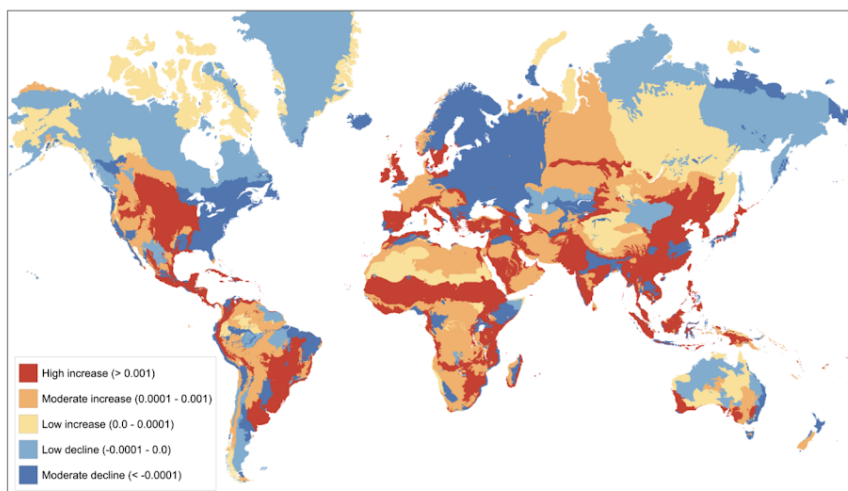
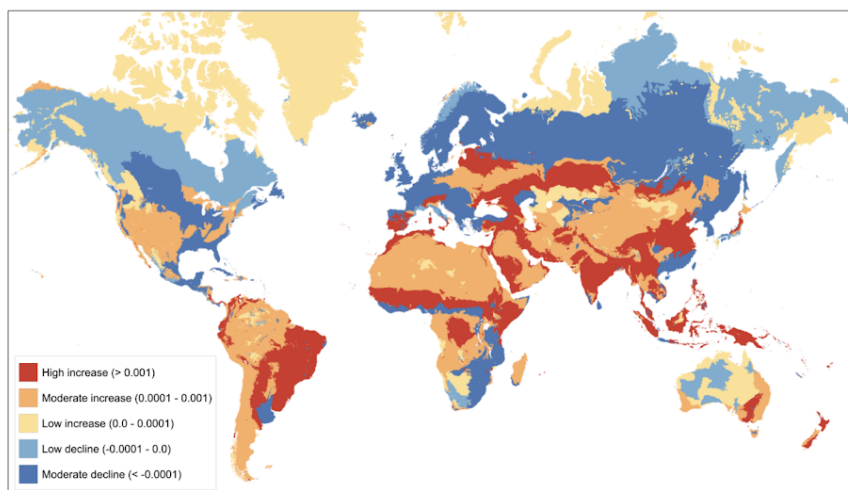
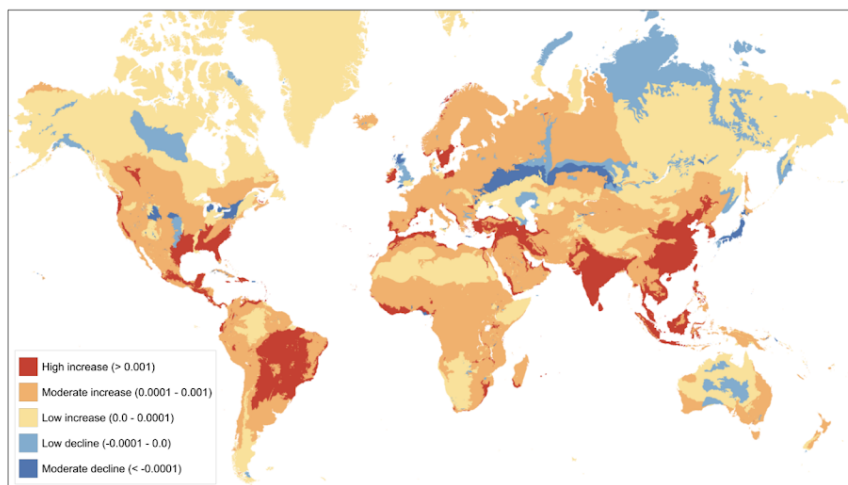
890



Figure captions

895

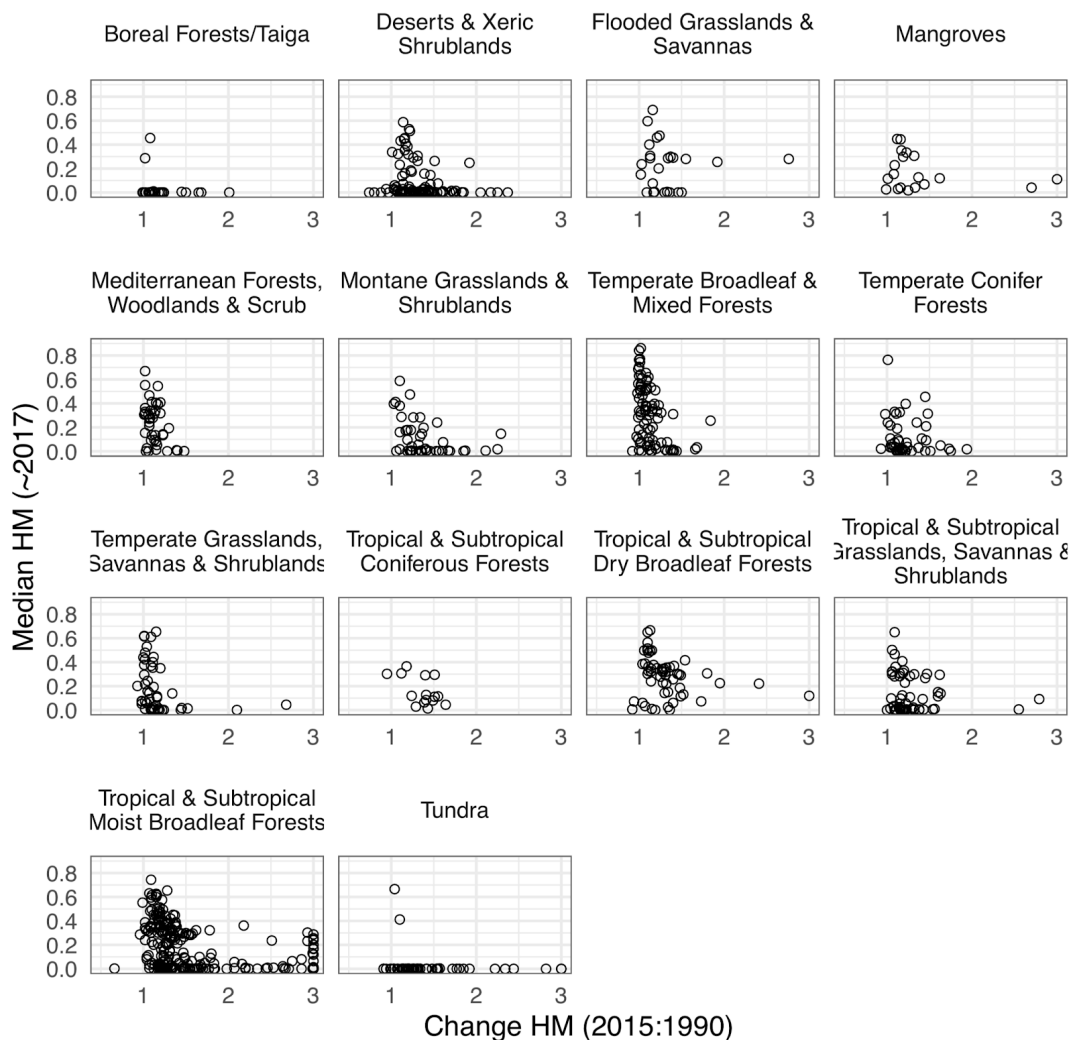
Figure 1. A comparison of the recent trends in human activities by ecoregion using the mean annualized difference estimated by: (a) human modification (H , from 1990-2015); (b) human footprint (for 1993-2009, Venter et al. 2016); and (c) temporal human pressure index (for ~1995-2010, Geldmann et al. 2019). Note: interactive maps are available at: <https://davidtheobald8.users.earthengine.app/view/global-human-modification-change>.





900

Figure 2. Graphs of the ratio of natural lands loss (2015:1990) and contemporary (~2017) degree of human modification (denoted as HM) for each of the 14 biomes and its ecoregions, globally. Note that ecoregions with change ratios ≥ 3.0 are placed on the maximum x-axis value (3.0).



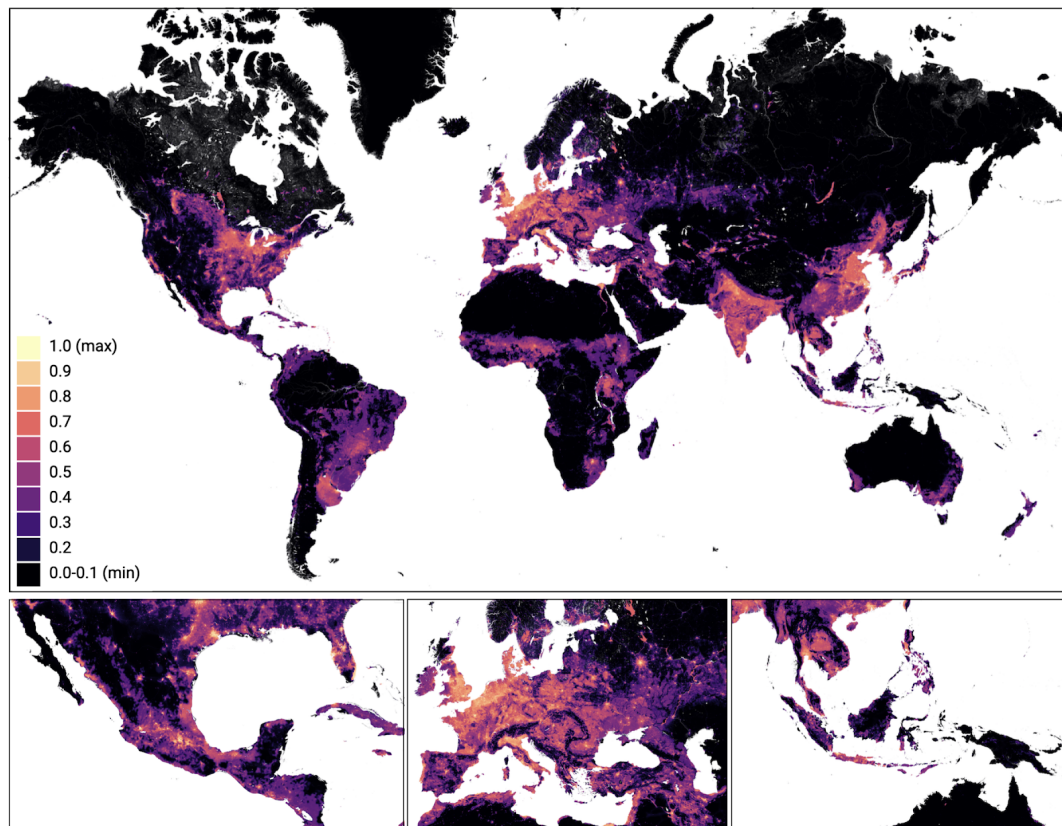
905



Figure 3. The degree of human modification for circa ~2017: (a) globally; (b) central America; (c) Europe, and (d) Oceania. Note: interactive maps are available at:

<https://davidtheobald8.users.earthengine.app/view/global-human-modification-change>.

910



915

920